Organic Electronics 14 (2013) 3109–3116

Contents lists available at ScienceDirect

Organic Electronics

journal homepage: www.elsevier.com/locate/orgel

Electrical and photoelectrical properties of P3HT/n-Si hybrid organic–inorganic heterojunction solar cells

V.V. Brus [a,b,*], M. Zellmeier [a], X. Zhang [a], S.M. Greil [a], M. Gluba [a], A.J. Töfflinger [a], J. Rappich [a], N.H. Nickel [a]

[a] Helmholtz-Zentrum Berlin für Materialien und Energie, Institut für Si-Photovoltaik, Kekuléstr. 5, 12489 Berlin, Germany
[b] Chernivtsi National University, Department of Electronics and Energy Engineering, Kotsubinsky str. 2, 58012 Chernivtsi, Ukraine

ARTICLE INFO

Article history:
Received 1 June 2013
Received in revised form 30 June 2013
Accepted 16 July 2013
Available online 2 August 2013

Keywords:
Hybrid solar cell
Heterojunction
Current transport
Quantum efficiency

ABSTRACT

A detail analysis of electrical and photoelectrical properties of hybrid organic–inorganic heterojunction solar cells poly(3-hexylthiophene) (P3HT)/n-Si, fabricated by spin-coating of the polymeric thin film onto oxide passivated Si(100) surface, was carried out within the temperature ranging from 283 to 333 K. The dominating current transport mechanisms were established to be the multistep tunnel-recombination and space charge limited current at forward bias and leakage current through the shunt resistance at reverse bias. A simple approach was developed and successfully applied for the correct analysis of the high frequency *C–V* characteristics of hybrid heterojunction solar cells. The P3HT/n-Si solar cell under investigation possessed the following photoelectric parameters: J_{sc} = 16.25 mA/cm^2, V_{oc} = 0.456 V, *FF* = 0.45, η = 3.32% at 100 mW/cm^2 AM 1.5 illumination. The light dependence of the current transport mechanisms through the P3HT/n-Si hybrid solar cells is presented quantitatively and discussed in detail.

1. Introduction

The interest in fundamental and applied research of conducting polymers as well as organic and hybrid organic/inorganic heterostructures has been rapidly increasing during the last decades [1–3].

Organic/inorganic hybrid heterojunctions merge advantages of both organic and inorganic semiconductors by unique combination of high quality electrical properties of inorganic materials with the film-forming properties of polymers. The fabrication of organic/inorganic hybrid semiconductor heterojunctions allows the development of a new class of semiconductor devices, which are very prospective for application in low cost flexible electronics, optoelectronics and photovoltaics.

However, in spite of many advantages of hybrid heterojunction solar cells, there are a few drawbacks which have to be overcome in order to fabricate stable hybrid heterojunction solar cells with the compatible efficiency comparing with conventional c-Si homojunction solar cells and high quality CdTe or $CuInSe_2$ thin film inorganic heterojunction solar cells [4]. One of the reasons of the relatively low efficiency of hybrid heterojunction solar cells is the lack of knowledge about electrical processes which take place in organic/inorganic heterojunction solar cells and thus determine their photoelectrical parameters.

There are many interesting works dedicated to the fabrication and analysis of new hybrid heterojunction solar cells based on different materials [5–12]. However, most of them are focusing on the design and configuration of organic/inorganic heterostructures in order to increase their photoelectric efficiency. At the same time much less attention is paid on the analysis of the dominating current transport mechanisms, DC and AC electrical properties as well as their dependence on different external conditions

* Corresponding author at: Chernivtsi National University, Department of Electronics and Energy Engineering, Kotsubinsky str. 2, 58012 Chernivtsi, Ukraine. Tel.: +380 66 4608294.
E-mail addresses: victorbrus@mail.ru, v.brus@chnu.edu.ua (V.V. Brus).

1566-1199/$ - see front matter © 2013 Elsevier B.V. All rights reserved.
http://dx.doi.org/10.1016/j.orgel.2013.07.021

that is very important for the operation of high quality optoelectronic devices. Therefore, a gap between the level of the efficiency of experimental hybrid solar cells and that of the understanding of physical and chemical processes exists. It is quite obvious that the gap has to be closed in order to create favourable conditions for the further development of high efficient hybrid heterojunction solar cells.

This paper reports the results of a detail analysis of DC and AC electrical as well as photoelectrical properties of planar hybrid heterojunction solar cells P3HT/n-Si within the temperature range from 283 to 333 K.

2. Experimental part

Single crystal n-doped Si(100) substrates ($\rho = 6\ \Omega$ cm, $n = 7.4 \times 10^{14}$ cm^{-3}) were ultrasonically cleaned in isopropanol and rinsed in deionized water ($\rho = 10^8\ \Omega$ cm). The substrates were etched in 5% HF solution during 5 min in order to eliminate the native oxide. Afterward, the freshly H-terminated Si(100) substrates have been oxidized under laboratory conditions ($T = 300$ K, $RH = 18\%$) for 10 h in order to obtain an oxide passivated Si(100) surface with low density of interface states [13]. The thickness of the SiO_2 layer d_{SiO2} amounts to about 2 nm as measured by means of an ellipsometer (SENTECH SE850).

The P3HT thin film was deposited onto oxide passivated Si substrates by spin-coating (2000 rpm, 30 s) of 2 mg P3HT solved in 5 ml 1-2-dichlorobenzene solution. Afterwards the P3HT/n-Si hybrid heterostructures were transferred to a vacuum chamber and annealed at 373 K and 10^{-7} mbar for 1 h. A semitransparent Au front contact was deposited by thermal evaporation. The back electrical contact to the n-Si(100) substrates was prepared outside the vacuum chamber by means of an In—Ga eutectic. The active area of the fabricated P3HT/n-Si hybrid solar cells was 0.2 cm^2.

The morphology of the surface of the P3HT thin film on the Si substrate and the cross-section of the heterostructure under investigation were analyzed by means of a scanning electron microscope (SEM) Hitachi S 4100. The structural properties of the P3HT/Si surface were inspected by using Raman spectroscopy (LabRAM micro Raman, Dilor, excitation wavelength 632.82 nm).

Current–voltage (I–V) characteristics of the P3HT/n-Si heterojunctions were measured by a high current source measuring unit Keithley 238 at different temperatures in the dark and under illumination. The temperature control was carried out by a thermal inducing vacuum platform ThermoChuck TP0315B. The light source was an AM1.5 solar simulator (Steuernagel). The capacitance–voltage (C–V) characteristic was measured by a Keithley 590 CV Analyzer at an AC frequency of 1 MHz at 293 K.

Optical properties of the P3HT thin film and semitransparent Au front contact were measured by a Perkin Elmer UV/VIS/NIR spectrometer Lambda 19 within the wavelength range from 300 to 1500 nm. The spectral distribution of the apparent quantum efficiency of the hybrid heterojunctions under investigation was measured using a monochromator SPEX 270 M within the wavelength region from 300 to 1150 nm. The calibration of the monochromator was carried out by means of a calibrating Si solar cell (Fraunhofer ISE CalLab PV Cells).

3. Results and discussions

3.1. Morphology and structural properties

The surface and the cross-section SEM images of a P3HT thin film spin-coated onto Si substrate are shown in Fig. 1 at the angle of 30°. It is seen that the polymer thin film is not uniform over the surface, mainly due to the high rotation velocity during the deposition that decorates stripes. However, any pinholes in the thin film were not observed. The thickness of the P3HT layer varies from 40 to 60 nm.

The Raman spectrum of the surface of the P3HT/Si hybrid heterostructure is shown in Fig. 2. The first three peaks 298 cm^{-1}, 520 cm^{-1} and 942 cm^{-1} originate from the Si substrate [14]. The two sharp peaks at 1378 cm^{-1} and 1442 cm^{-1} and the small one at 1512 cm^{-1} result from the C—C stretching vibrations and C=C skeleton stretching of the thiophene rings, respectively. The small and broad peak at about 2886 cm^{-1} (see inset in Fig. 2) is observed as a result of the CH_2 symmetric and antisymmetric stretching vibrations [15].

3.2. Electrical properties

The prepared P3HT/n-Si hybrid heterojunctions possessed sharply defined rectifying properties within the measured temperature range (Fig. 3) that provides evidence in the formation of a high quality electric junction at the polymer/semiconductor interface.

Fig. 4 shows the forward branches of the I–V characteristics of the hybrid heterojunctions under investigation at different temperatures. The height of the potential barrier φ_0 of the P3HT/n-Si heterojunction can be estimated by means of the extrapolation of the linear segments of the forward I–V characteristics toward the interception with the voltage axis. The temperature dependence of the estimated height of the potential barrier of the P3HT/n-Si heterojunctions is well governed by the linear equation:

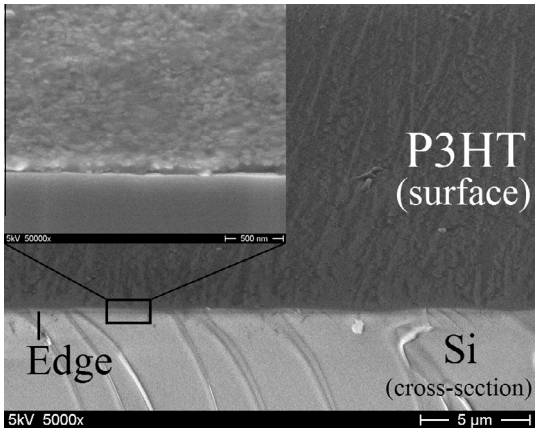

Fig. 1. SEM images of the spin-coated P3HT thin film onto Si substrate.

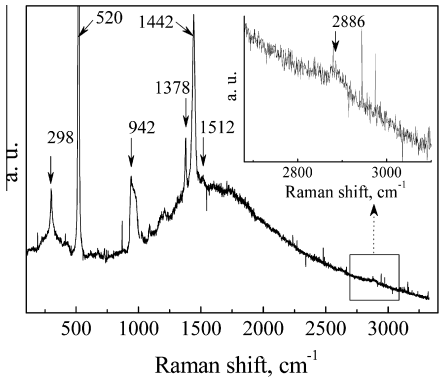

Fig. 2. Raman spectrum of the P3HT/Si heterostructure.

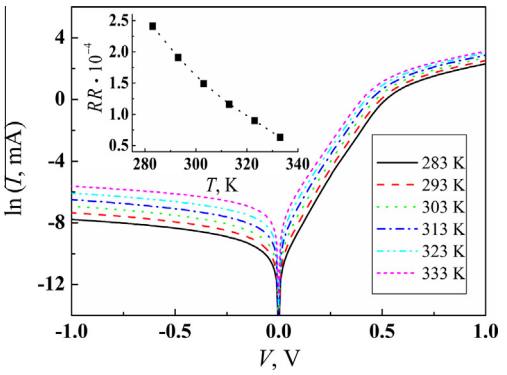

Fig. 3. *I–V* characteristics of the P3HT/n-Si solar cells measured at different temperatures. The inset shows the temperature dependence of the rectification ratio *RR* calculated at 1 V.

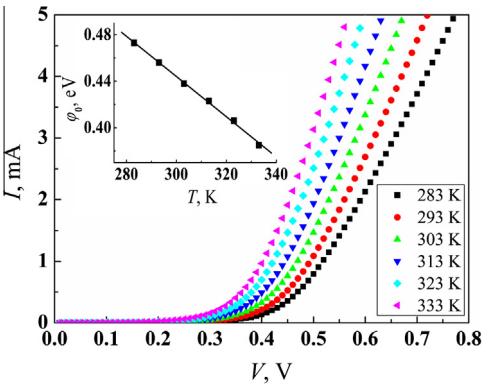

Fig. 4. Forward branches of the *I–V* characteristics of the P3HT/n-Si solar cells. Temperature dependence of the height of the potential barrier is shown in the inset.

$$\varphi_0(T) = qV_{bi}(T) = \varphi_0(0) - \beta_\varphi \cdot T, \quad (1)$$

where V_{bi} is the built-in voltage, $\beta_\varphi = 1.76 \times 10^{-3}$ eV K^{-1} is the temperature coefficient of the height of the potential barrier, $\varphi_0(0) = 0.96$ eV is the value of the height of the potential barrier at $T = 0$ K. It is worth noting that the interface states strongly effect on barrier and thus on electrical properties of the hybrid heterojunction solar cells under investigation, since the temperature coefficient of the height of the potential barrier β_φ is one order larger than that of the Si band gap $\beta_{Eg(Si)} = 2.3 \times 10^{-4}$ eV K^{-1} [16]. Si is the narrow band gap component of the P3HT/Si heterojunction and should determine the temperature dependence of φ_0 in the absence of electrically active interface states.

The voltage dependences of the differential resistance R_{dif} of the forward biased hybrid heterojunction solar cells under investigation are shown in Fig. 5.

The DC equivalent circuit of our hybrid heterojunction solar cells can be represented by three resistors connected in series (see inset in Fig. 5), where R_d is the resistance of the space charge region, R_{P3HT} is the resistance of the polymer layer and front electric contact, R_s is the voltage independent series resistance, which is determined by the sum of the resistances of the quasi neutral region, back contact as well as contacting wires. At low forward bias the resistance of the depletion region is the dominating one. It is seen by the exponential decrease in the differential resistance with the increasing forward bias (linear segments at low bias in Fig. 5).

If the applied forward bias is higher than the built-in voltage the width of the depletion region becomes negligibly small and, thus R_d, which does not limit the forward current under these conditions. However, in the contrary of inorganic Schottky diodes and heterojunctions [17,18], the differential resistance R_{dif} of the hybrid organic–inorganic solar cells under investigation does not become saturated at forward bias $V > V_{bi}$ (Fig. 5). The reason is the voltage dependent resistance R_{P3HT}, since series resistance $R_s = 5\ \Omega$ and does not depend on applied voltage. The strong decrease in the differential resistance at fixed forward bias R_{dif}(0.8 V) with the rise of temperature, shown in the inset of Fig. 5, also provides evidence that the series resistance R_s is not a dominating one. The only temperature dependent component of the series resistance is the resistance of the quasi neutral region (the Si layer between the edge of the depletion region and back contact). All shallow donors in the n-Si substrates under investigation are ionized within our temperature range. At the same time

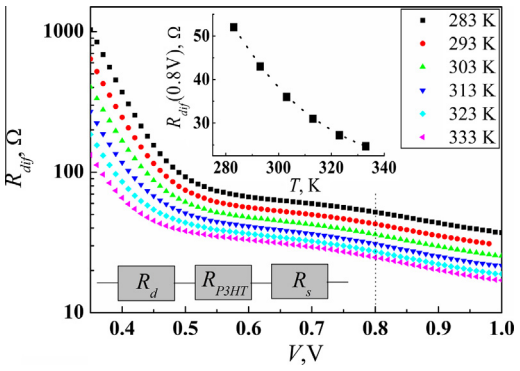

Fig. 5. Dependence of the differential resistance of the P3HT/n-Si hybrid heterojunction solar cells on applied forward biases. The insets show the temperature dependence of the differential resistance at a fixed forward bias of 0.8 V and DC equivalent circuit, respectively.

the intrinsic concentration is much lower than the doping level even at our maximum temperature of 333 K $n_i = (N_c N_v)^{1/2}\exp(-E_{g(Si)}/2kT) = 8.17 \times 10^{10}$ cm^{-3}, $n = 7.4 \times 10^{14}$ cm^{-3}. Therefore, the resistance of the quasi neutral region, in the contrary to the temperature dependence shown in the inset of Fig. 5, should even slightly increase with the rise of temperature because of the decrease in the mobility of electrons [16]. The voltage dependence of R_{P3HT} shows the deviation from the ohmic current transport mechanism through the P3HT thin film at forward bias $V > V_{bi}$, which will be discussed later in this paper.

Fig. 6 shows the I–V characteristics of the P3HT/n-Si solar cells at initial forward bias $V < V_{bi}$ in the semi logarithmical plot (positive potential "+" is applied to the P3HT thin film). It is seen that the measured I–V characteristics are exponential functions that correlates with the voltage dependence of R_{dif} at initial forward bias (Fig. 5).

The small forward bias $3kT/q < V < V_{bi}$ and the temperature independent slope $\Delta\ln(I)/\Delta V$ of the linear I–V characteristics in the semi logarithmical scale provide evidence that the current transport through the hybrid heterojunction solar cells under investigation is governed by the tunnel-recombination processes via interface states [19,20]. As it was mentioned above our hybrid heterojunctions are forward biased if the positive potential "+" is applied to the P3HT layer and the negative "−" to the Si substrate. In this case the external electric field enhances the injection and tunneling of electrons from n-Si to unoccupied energy levels created by surface states at the heterojunction interface and defects in P3HT. However, it should be mentioned that P3HT is a conjugated polymer with hole conductivity. Therefore, electrons cannot move further through the P3HT layer toward the anode (front Au electrode at forward bias). At the same time externally applied electric field promotes the injection of holes from the Au contact. The hole injection from the Au electrode into the P3HT layer is the result of the ionization of molecules located close to the surface of the metallic anode and the tunneling transition of an electron from the higher occupied molecular orbital (HOMO) to a free electronic level in the metal. It is worth to note that the effect of the imaging force at the metal surface results in the much higher probability of the ionization of organic molecules near the gold/P3HT interface comparing with that in the bulk P3HT at the same strength of the applied electric field [21,22]. The injected holes drift through the P3HT thin film and finally recombine with the electrons from the Si substrate via deep energy levels in the vicinity of the P3HT/n-Si heterojunction interface.

The I–V curves shown in Fig. 6 are well described by the following equation [20]:

$$I = I_{00}\exp[\beta T]\exp[AV], \tag{2}$$

where the experimental values of the constants are $I_{00} = 5.1 \times 10^{-11}$ mA, $\beta = 4.6 \times 10^{-2}$ K^{-1}, $A = 21$ V^{-1}. It is known that the value of the constant β depends on the temperature coefficient of the height of the potential barrier β_φ as follows [20,23]:

$$\beta = A\frac{dV_{bi}}{dT} = qA\beta_\varphi, \tag{3}$$

The calculated value of the constant β, using Eq. (3), is equal to 3.7×10^{-2} K^{-1} that is in good correlation with its experimentally determined value from the slope of the linear temperature dependence shown in the inset of Fig. 6.

If the applied forward bias V increases further the deviation from the strong exponential I–V dependence occurs (see Fig. 3). The measured I–V curves of the P3HT/n-Si hybrid heterojunctions can be described by the power dependence I–V^m at large forward bias $V > V_{bi}$, where the power m slightly depends on temperature (see Fig. 7).

The power dependence I–V^m with $m > 2$ provides evidence that the dominating current transport mechanism through the P3HT/n-Si heterojunction solar cells at forward bias $V > V_{bi}$ is determined by the space charge limiting current through the P3HT layer in the presence of the high density of trapping states distributed over the polymer's "band gap" [24–26]. When traps are present most of the injected holes may be localized and will not contribute to the current flow and the I–V characteristic will be determined by the energy distribution of the trapping states as well as on the injection level. This model is in a

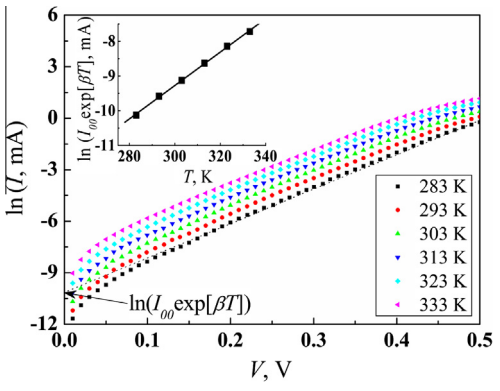

Fig. 6. The I–V characteristics of the P3HT/n-Si solar cells at different temperatures and low forward bias. The temperature dependence of the cut-off current $I_{00}\exp[\beta T]$ is shown in the inset.

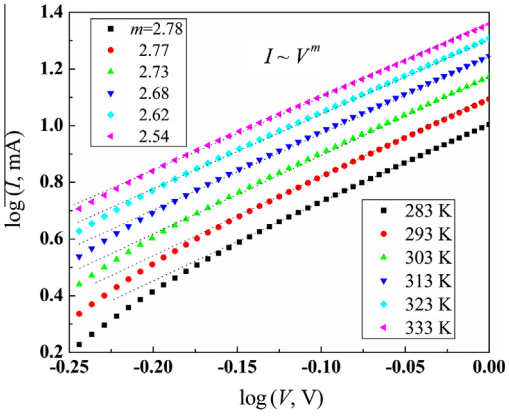

Fig. 7. I–V characteristics of the P3HT/n-Si solar cells at large forward bias plotted in the logarithmical scale.

good agreement with the reported high trap density (over 10^{16} cm^{-3}) in as-spin-coated P3HT thin films [27].

However, the behavior of the Au/P3HT contact is not entirely clear up to now as well as its effect on the measured *I–V* characteristics at large forward bias. This question deserves additional investigations and comparison with other metal/P3HT contacts [28].

At reverse bias the electric current through the P3HT layer is carried by the small number of holes injected from the Si substrate (holes are the minority charge carriers in n-Si), therefore its resistance becomes much higher comparing to that at forward bias. The reverse *I–V* characteristics of the P3HT/n-Si hybrid solar cells are linear within the voltage range $3kT/q < V < 4$ V at all temperatures (see Fig. 8). It is seen the exponential dependence of the reverse current at fixed applied voltage (see inset in Fig. 8) I_{rev} - $\sim \exp[-\Delta E_a/kT]$ with the activation energy $\Delta E_a = 0.34$ eV. This kind of reverse *I–V* characteristics can result from the leakage current through the shunt resistance of the space charge region or be governed by the thermally exited charge carriers hopping mechanism in the P3HT layer [16].

If the hopping mechanism is the dominating one for the charge carriers' transport at reverse bias, it means that the P3HT layer would limit the reverse current and thus the major part of the applied voltage would drop over the polymeric layer. The capacitive behavior of pure (undoped) polymeric thin films is the same as that of dielectric layers [29]. In this case the measured high frequency capacitance C_m should be voltage independent. However, the measured high frequency (1 MHz) capacitance C_m of our hybrid solar cells shows voltage dependence (see Fig. 9) indicating that the reverse voltage drops over the space charge region [16]. Therefore, the reverse current transport mechanism is determined by the leakage current through the shunt resistance of the depletion region.

It is known that the measured capacitance C_m of semiconductor heterojunctions depends on many parameters such as series R_s and shunt R_s resistance and interface states N_{ss} [30–32]. Therefore, the measured capacitance of non-ideal heterojunction solar cells cannot be used in order to determine the built-in voltage and doping concentration without appropriate correction.

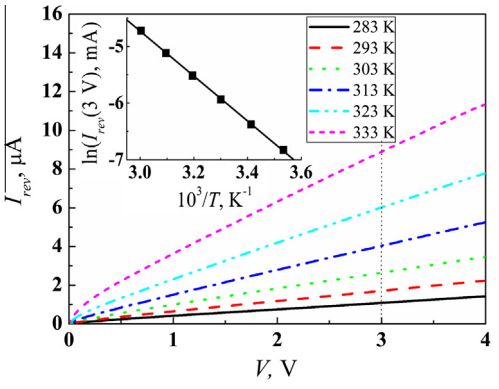

Fig. 8. Reverse *I–V* characteristics of the P3HT/n-Si heterojunctions. The inset shows the Arrhenius plot of the reverse current at a fixed applied bias of 3 V.

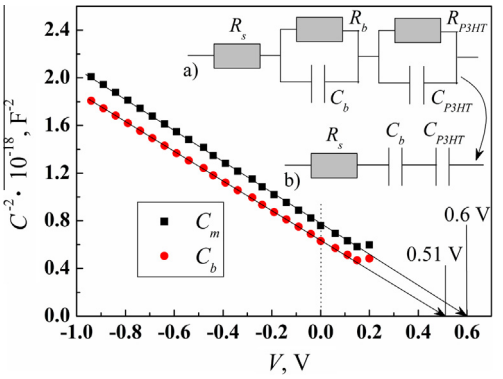

Fig. 9. Mott-Schottky plots for the measured capacitance C_m (rectangles) and barrier capacitance C_b (circles) of the P3HT/n-Si hybrid heterojunction solar cells measured at 1 MHz and 293 K. The inset (a) shows the high frequency equivalent circuit of our hybrid solar cells. The simplified equivalent circuit, which takes into account the following inequalities $R_b \gg 1/\omega C_b$ and $R_{P3HT} \gg 1/\omega C_{P3HT}$, is shown in the inset (b).

The *C–V* characteristics of the P3HT/n-Si hybrid solar cells were measured at the high frequency of AC signal $f = 1$ MHz in order to eliminate the effect of the additional capacitance C_{ss}, which results from the charging and discharging of interface states, since they cannot follow the high frequency signal. The high frequency equivalent circuit of our hybrid solar cells is shown in the inset (a) of Fig. 9, where the barrier capacitance C_b (the voltage dependent capacitance of the space charger region) and the geometrical capacitance of the P3HT thin film C_{P3HT} are given by the following equations, respectively:

$$C_b = S\sqrt{\frac{q\varepsilon_0\varepsilon_{Si}N_D}{2(V_{bi}-V)}}, \tag{4}$$

$$C_{P3HT} = \frac{\varepsilon_0\varepsilon_{P3HT}S}{d}, \tag{5}$$

where ε_0 is the permittivity of vacuum, $\varepsilon_{Si} = 11.9$ and $\varepsilon_{P3HT} = 3$ are the dielectric constants of silicon and P3HT, respectively, $d = 50$ nm is the average thickness of the P3HT layer.

In our case the following inequalities are valid $R_b \gg 1/\omega C_b$ and $R_{P3HT} \gg 1/\omega C_{P3HT}$ at reverse and small forward bias, where $\omega = 2\pi f$ is the angular frequency. It means that the reactive capacitance resistances shunt the appropriate active resistors and thus the AC-characteristics of our P3HT/n-Si solar cells under reverse biases can be successfully analyzed in the scope of the equivalent circuit shown in the inset (b) of Fig. 9 (a series resistance R_s in series with the barrier capacitance C_b and the geometrical capacitance of the P3HT layer C_{P3HT}). The series resistance R_s was established to be equal to 12 Ω, it is twice higher than its value for the DC measurements, since another sample holder was used during *C–V* measurements.

Therefore, the expression for the measured impedance of the equivalent circuit under consideration in order to take into account the effect of the series resistor R_s can be written as:

$$Z = R_s - i\frac{1}{\omega C_{eq}} = Z' - iZ'', \tag{6}$$

where Z' and Z'' are the real and imaginary components of the measured impedance, respectively, C_{eq} is the equivalent capacitance:

$$C_{eq} = \frac{C_b C_{P3HT}}{C_b + C_{P3HT}}, \tag{7}$$

Therefore, the measured capacitance of the P3HT/n-Si hybrid solar cell is given by the following equation:

$$C_m = -\frac{1}{\omega}\frac{Z''}{Z'^2 + Z''^2} = \frac{C_{eq}}{1 + \omega^2 R_s^2 C_{eq}^2}, \tag{8}$$

It is now easy to see that expression (8) is a quadratic equation. Therefore, the expression for the equivalent capacitance C_{eq} is given by the following formula (in our case another solution of Eq. (8) does not provide physically based values for C_{eq}):

$$C_{eq} = \frac{1 - \sqrt{1 - 4\omega^2 R_s^2 C_m^2}}{2\omega^2 R_s^2 C_m}, \tag{9}$$

Considering Eqs. (7) and (9) we can write the expression for the actual barrier capacitance of the P3HT/n-Si hybrid solar cells as:

$$C_b = \frac{\varepsilon_0 \varepsilon_{P3HT} S\left(1 - \sqrt{4\omega^2 R_s^2 C_m^2}\right)}{2\varepsilon_0 \varepsilon_{P3HT} \omega^2 R_s^2 C_m S - d\left(1 - \sqrt{4\omega^2 R_s^2 C_m^2}\right)}. \tag{10}$$

The actual Mott–Schottky plot C_b^{-2} vs. V is shown in Fig. 9 (circles). The corrected C–V characteristic is valid for the determination of the built-in voltage V_{bi} by the extrapolation of the linear dependence toward the interception with the voltage axis as well as the doping concentration N_D and thus the concentration of free electrons in the Si substrate n, since high quality Si single crystal is not a compensated semiconductor, from the slope of the C_b^{-2} vs. V dependence [16]:

$$N_D = \frac{2}{q\varepsilon_0 \varepsilon_{Si} S^2 \frac{\Delta C_b^{-2}}{\Delta V}}. \tag{11}$$

The determined values for the built-in voltage $V_{bi} = 0.51$ V and the doping concentration $N_D = 7.6 \times 10^{14}$ cm^{-3} from the corrected C–V characteristic are well correlated with their values determined from the DC measurements at the same temperature. The slightly higher values of V_{bi} and N_D determined from the AC measurements may result from the presence of an electric charge trapped at the heterojunction interface [16].

3.3. Photoelectrical properties

The I–V characteristic of a P3HT/n-Si hybrid solar cell is shown in Fig. 10 as well as the main photoelectric parameters measured under the AM 1.5 illumination conditions at 293 K.

The forth quadrant ($V_{oc} \geqslant V \geqslant 0$) of the light I–V characteristic is the most important, since it determines all photoelectrical parameters. Taken into account the dominating current transport mechanism through our hybrid solar cells at forward biases $V < V_{oc}$ (2), we can write the expression for the I–V characteristic under illumination (within forth quadrant) considering the effect of the series R_s and shunt R_{sh} resistance:

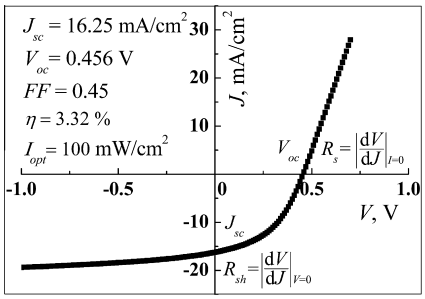

Fig. 10. I–V characteristic of the P3HT/n-Si hybrid heterojunction solar cells under illumination (100 mW/cm^2, AM 1.5).

$$J = J_0 \exp[A(V - JR_s)] + \frac{V - JR_s}{R_{sh}} - J_{ph}, \tag{12}$$

where $J_0 = J_{00}\exp(\beta T)/S$ is the cut-off current density, $R_s = 8.6\ \Omega\ \text{cm}^2$ and $R_{sh} = 127\ \Omega\ \text{cm}^2$ were determined from the I–V characteristic under illumination (see Fig. 10) [33], J_{ph} is the photocurrent which cannot be measured experimentally in the presence of series resistance. The expressions for the short-circuit and open-circuit conditions under illumination are given by the following equations, respectively:

$$-J_{sc} = J_0 \exp[AJ_{sc}R_s] + \frac{J_{sc}R_s}{R_{sh}} - J_{ph}, \tag{13}$$

$$0 = J_0 \exp[AV_{oc}] + \frac{V_{oc}}{R_{sh}} - J_{ph}. \tag{14}$$

If we express J_{ph} from Eq. (14) and insert the result in (13) the following transcendental equation will be obtained:

$$TE = J_{sc} - J_0(\exp[AV_{oc}] - \exp[AJ_{sc}R_s]) - \frac{V_{oc} - J_{sc}R_s}{R_{sh}} = 0. \tag{15}$$

Eq. (15) can be used in order to calculate either short-circuit current density J_{sc} or open-circuit voltage V_{oc} of the P3HT/n-Si hybrid solar cells under investigation. Let us do this calculation using the previously determined values for parameters J_0 and A, which were determined from the dark I–V characteristic measured at the same temperature, in order to show if their values are valid under light conditions or not.

It is seen from Fig. 11 that the calculated value of the open-circuit voltage V_{oc} is larger than its experimental value as well as the built-in voltage at 293 K. The calculated short-circuit current I_{sc} is considerably smaller than the measured value (see Fig. 10). The values of the parameters I_{sc}, V_{oc}, R_s and R_{sh} used in our calculations are valid since all of them were determined from the I–V characteristic under illumination. Therefore, the values of the parameters J_0 and A, which quantitatively describe the current transport through our hybrid heterojunctions at low forward bias, determined under dark conditions (see Fig. 6) are not valid for the analysis of the photoelectrical properties. It means

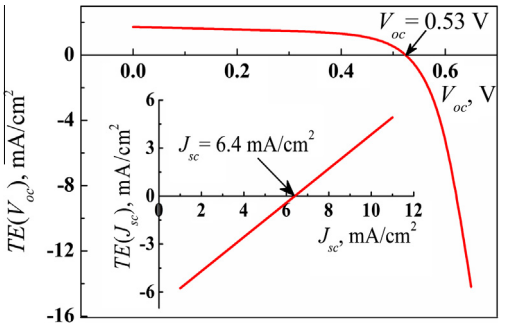

Fig. 11. The calculation of the open-circuit voltage V_{oc} and short-circuit current I_{sc} of the P3HT/n-Si heterojunction solar cells using parameters J_0 and A determined under dark conditions at 293 K.

that the conditions of the current transport through the P3HT/n-Si hybrid solar cells are light dependent as in the case of many inorganic heterojunction solar cells [34–36]. The observed light dependence of the tunnel-recombination current transport mechanism can be caused by the absorption of incident light by interface and bulk states in the vicinity of P3HT/Si interface. The values of coefficients J_0 and A under illumination differ from their values determined under dark conditions due to the recharging interface states and traps within the space charge region [35]. It is known that coefficient A depends on the shape and height of potential barrier and coefficient J_0 is proportional to the density of interface states [19,20]. Since interface states, as usually, create both shallow and deep levels within band gap, the charge state of heterojunction interface and, thus, coefficients J_0 and A depend on illumination conditions [13,32].

The dominating current transport mechanisms must be determined under illumination in order to carry out the correct quantitative analysis of the photoelectric properties of the P3HT/n-Si hybrid solar cells. However, this research goes beyond the scope of this paper and will be carried out in future.

The spectral distribution of the apparent quantum efficiency of the P3HT/n-Si heterojunction solar cells was measured as the ratio of the number of charge carriers, which form the short circuit current to the number of incident photons of a given energy on the solar cell per unit time. The normalized spectral distribution of the apparent quantum efficiency measured at 293 K is shown in Fig. 12.

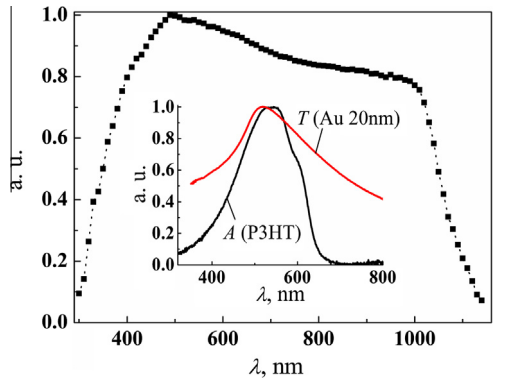

Fig. 12. The normalized spectrum of the apparent quantum efficiency of the P3HT/n-Si hybrid solar cells. The normalized spectra of the transmittance of the semitransparent front Au contact and the absorption of the P3HT thin film are shown in the inset.

The energy location of the long wavelength edge is well correlated with the band gap of the Si substrate. The increase of the quantum efficiency within the spectral range from 400 to 600 nm results from the higher transmittance of the semitransparent gold contact as well as from the contribution in photocurrent by the P3HT layer, which possesses the absorption maximum within the mentioned spectral range (see inset in Fig. 12).

4. Conclusions

Organic/inorganic hybrid heterojunction solar cells P3HT/n-Si were fabricated by means of the spin-coating of P3HT thin films onto oxide passivated Si(100) substrates. The prepared P3HT/n-Si hybrid heterojunctions possessed sharply defined rectifying properties within the measured temperature range from 283 to 333 K.

The linear temperature dependence of the height of the potential barrier of the P3HT/n-Si hybrid heterojunction was shown. The current transport through the organic/inorganic solar cells under dark conditions is determined by the tunnel-recombination processes via interface states and space charge limited currents at forward bias as well as leakage current through the shunt resistance of the depletion region at reverse bias. The domination of tunnel-recombination mechanism at low forward bias results from the high density of interface states at the P3HT/Si heterojunction interface. Therefore, the surface recombination is the main efficiency limiting factor in our hybrid heterojunction solar cells.

A simple approach was developed and successfully applied for the correct analysis of the high frequency C–V characteristics of the P3HT/n-Si hybrid heterojunction solar cells. The values of the built-in voltage and doping concentration determined from the high frequency C–V characteristic were in good agreement with their values determined from the DC measurements.

The P3HT/n-Si solar cell under investigation lead to the following photoelectric parameters: J_{sc} = 16.25 mA/cm^2, V_{oc} = 0.456 V, FF = 0.45, η = 3.32% at 100 mW/cm^2 AM 1.5 illumination.

The expression for the I–V characteristic of the P3HT/n-Si hybrid solar cells under illumination within the forth quadrant was derived. The light dependence of the current transport mechanisms through the hybrid solar cells under investigation was quantitatively shown.

References

[1] M. Wright, A. Uddin, Organic–inorganic hybrid solar cells: a comparative review, Solar Energy Materials and Solar Cells 163 (2012) 87–111.
[2] J. Chandrasekaran, D. Nithyaprakash, K.B. Ajjan, S. Maruthamuthu, D. Manoharan, S. Kumar, Hybrid solar cells based on blending of organic and inorganic materials – an overview, Renewable and Sustainable Energy Reviews 15 (2011) 1228–1238.

[3] P.G. Nicholson, F.A. Castro, Organic phtovoltaics: principles and techniques for nanometre scale characterization, Nanotechnology 21 (2010) 26. 492001.
[4] T.M. Razykov, C.S. Ferekides, D. Morel, E. Stefanakos, H.S. Ullal, H.M. Upadhyaya, Upadhyaya solar photovoltaic electricity: current status and future prospects, Solar Energy 85 (2011) 1580–1608.
[5] X. Shen, B. Sun, D. Liu, S.-T. Lee, Hybrid heterojunction solar cell based on organic–inorganic silicon nanowire array architecture, Journal of the American Chemical Society 133 (2011) 19408–19415.
[6] C.-Y. Liu, Z.C. Holman, U.R. Kortshage, Hybrid solar cells from P3HT and silicon nanocrystals, Nano Letters 9 (2009) 449–452.
[7] M. Bredol, K. Matras, A. Szatkowski, J. Sentra, A. Prodi-Schwab, Prodi-Schwab P3HT/ZnS: a new hybrid bulk heterojunction photovoltaic system with very high open circuit voltage, Solar Energy Materials and Solar Cells 93 (2009) 662–666.
[8] A.K.K. Kyaw, X.W. Sun, C.Y. Jiang, G.Q. Lo, D.W. Zhao, D.L. Kwong, An inverted organic solar cell employing a sol–gel derived ZnO electron selective layer and thermal evaporated MoO_3 hole selective layer, Applied Physics Letters 93 (2008) 221107.
[9] Y. Li, E.D. Peterson, H. Hung, M. Wang, D. Xue, W. Nie, W. Zhou, D.L. Carroll, Tube-based geometries for organic photovoltaics, Applied Physics Letters 96 (2010) 243505.
[10] D.C. Olson, S.E. Shaheen, M.S. White, W.J. Mitchell, M. Hest, R.T. Collins, D.S. Cinley, Band-offset engineering for enhanced open-circuit voltage in polymer-oxide hybrid solar cells, Advanced Functional Materials 17 (2007) 264–269.
[11] L.-C. Chen, C.-C. Wang, C.-B. Cheng, Influence of dopant and polymeric matrix on Indium tin oxide/p-zincphtalocyanine/n-Si hybrid solar cells, Thin Solid Films 517 (2009) 1790–1793.
[12] K. Yang, C. Xu, L. Huang, L. Zou, H. Wang, Hybrid nanostructure heterojunction solar cells fabricated using vertically aligned ZnO nanotubes grown on reduced praphene oxide, Nanotechnology 22 (2011) 405401.
[13] E.H. Nicollian, A. Goetzberger, The $Si–SiO_2$ interface-electrical properties as determined by the metal–insulator–silicon conductance technique, The Bell System Technical Journal 46 (1966) 1055–1133.
[14] I.D. Wolf, Micro-Raman spectroscopy to study local stress in silicon integrated circuits, Semiconductor Science and Technology 11 (1996) 139–154.
[15] V. Saini, Z. Li, S. Bourdo, E. Dervishi, Y. Xu, X. Ma, V. Kunets, G. Salamo, T. Viswanathan, A.R. Biris, D. Saini, A.S. Biris, Electrical, optical and morphological properties of P3HT-MWNT nanocomposites prepared by in situ polymerization, Journal of Physical Chemistry C 113 (2009) 8023–8029.
[16] S.M. Sze, Kwok K. NG, Physics of Semiconductor Devices, Wiley, New Jersey, 2007.
[17] L.A. Kosyachenko, X. Mathew, V.V. Motushchuk, V.M. Sklyarchuk, Electrical properties of electrodeposited CdTe photovoltaic devices on metallic substrates: study using small area Au–CdTe contacts, Solar Energy 80 (2006) 148–155.
[18] V.V. Brus, M.I. Ilashchuk, Z.D. Kovalyuk, P.D. Maryanchuk, K.S. Ulyanytsky, Electrical and photoelectrical properties of photosensitive heterojunctions $n\text{-}TiO_2/p\text{-}CdTe$, Semiconductor Science and Technology 26 (2011) 125006.
[19] A.R. Riben, D.L. Feucht, NGe–pGaAs heterojunctions, Solid-State Electronics 9 (1966) 1055–1065.
[20] A.R. Riben, D.L. Feucht, Electrical transport in nGe–pGaAs heterojunctions, International Journal of Electronics 20 (1966) 583–599.
[21] N.S. Averkiev, V.A. Zakrevskii, I.V. Rozhanskii, N.T. Sudar, Injection of holes into organic molecular solids, Physics of the Solid State 51 (2009) 910–916.
[22] N.S. Averkiev, V.A. Zakrevskii, I.V. Rozhansky, N.T. Sudar, Peculiarities of holes injection into organic molecular solids, Applied Physics Letters 94 (2009) 233308.
[23] A.M. Mancini, A. Valentini, L. Vasanelli, A. Losacco, Electrical properties of ZnO/CdTe heterojunctions, Journal of Crystal Growth 72 (1985) 530–537.
[24] P. Mark, W. Helfrich, Space-charge-limited currents in organic crystals, Journal of Applied Physics 33 (1962) 205–215.
[25] M.A. Lampert, P. Mark, Current Injection in Solids, Academic Press, New York, 1970.
[26] J.M. Montero, J. Bisquert, G. Garcia-Belmonte, E.M. Barea, H.J. Bolink, Trap-limited mobility in space-charge limited current in organic layers, Organic Electronics 10 (2009) 305–312.
[27] J. Schafferhans, A. Baumann, C. Deibel, V. Dyakonov, Trap distribution and the impact of oxygen-induced traps on the charge transport in poly(3-hexylthiophene), Applied Physics Letters 93 (2008) 093303.
[28] B. Reeja-Jayan, A. Manthiram, Influence of polymer–metal interface on the photovoltaic properties and long-term stability of $nc\text{-}TiO_2$-P3HT hybrid solar cells, Solar Energy Materials and Solar Cells 94 (2010) 907–914.
[29] C.H. Kim, O. Yaghmazadeh, D. Tondelier, Y.B. Jeong, Capacitive behavior of pentacene-based diodes: quasistatic dielectric constant and dielectric strength, Journal of Applied Physics 109 (2011) 083710.
[30] P. Chattopadhyay, D.P. Haldar, Capacitance–voltage characteristic of anisotype heterojunction in the presence of interface states and series resistance, Applied Surface Science 171 (2001) 207–212.
[31] V.V. Brus, On impedance spectroscopy analysis of nonideal heterojunctions, Semiconductor Science and Technology 27 (2012) 035024.
[32] V.V. Brus, The effect of interface state continuum on the impedance spectroscopy of semiconductor heterojunctions, Semiconductor Science and Technology 28 (2013) 025013.
[33] D.K. Schroder, Semiconductor Materials and Device Characterization, Wiley, New Jersey, 2006.
[34] J.R. Sites, H. Tavakolian, R.A. Sasala, Analysis of apparent quantum efficiency, Solar Cells 29 (1990) 39–48.
[35] M. Kontges, R. Reineke-Koch, P. Nollet, J. Beier, R. Schaffler, J. Parisi, Light induced changes in the electrical behaviour of CdTe and $Cu(In, Ga)Se_2$ solar cells, Thin Solid Films 403–404 (2002) 280–286.
[36] V.V. Brus, M.I. Ilashchuk, Z.D. Kovaluyk, P.D. Maryanchuk, Light-dependent *I–V* characteristics of $TiO_2/CdTe$ heterojunction solar cells, Semiconductor Science and Technology 27 (2012) 055008.